

Comparative Analysis of Different Hip Implants within a Realistic Human Model Located Inside a 1.5T MRI Whole Body RF Coil

Mikhail Kozlov, *Member, IEEE*, Gregory M. Noetscher *Member, IEEE*, Ara Nazarian, and Sergey N. Makarov, *Senior Member, IEEE*

Abstract— Temperature rise in surrounding tissues of a large orthopedic metallic implant subject to MRI is a significant point of concern today. Numerical electromagnetic and thermal modeling offers a way to model this complex problem with a sufficient degree of accuracy. We developed a workflow for realistic implant modeling, which includes an MRI coil, a multi-tissue human model, and accurately registered hip implants. We also obtained differences in the power loss density rises generated due to the presence of three hip implants placed in a phantom or a realistic human model, located inside a 1.5 T coil.

I. INTRODUCTION

Annually, millions of metallic orthopaedic devices are implanted in patients worldwide. Many of these patients require further medical care at some point in their life time post-implantation. As part of their medical regimen, a portion of these patients are subjected to magnetic resonance imaging (MRI) during the diagnostic phase of their care. Currently, very limited information is available on the effect of MRI imaging on adjacent orthopaedic implants and surrounding tissues. Of note is the issue of increased temperature in tissues adjacent to metallic implants in the body and the potential detrimental effect of such temperature gradients on the health of otherwise normal surrounding tissues. As a result, robust methodologies to properly model and simulate such temperature gradients are of great importance to further optimize imaging studies and patient care protocols for this population.

There are a variety of significant concerns related to temperature rise in surrounding tissue of a large orthopedic metallic implant subject to MRI [1], [2]. This rise needs to be calculated carefully for the patient's safety. The American Society for Testing and Materials (ASTM) released an ASTM F2182-11a standard [1] that defines the necessary test method for measurement of radio frequency (RF) induced heating on or near passive implants. This standard defines a homogeneous rectangular ($650 \times 420 \times 90$ mm) phantom filled by high conductivity media with a relative dielectric

M. Kozlov is with the Department of Neurophysics at the Max Plank Inst. for Human Cognitive and Brain Sciences in Leipzig, Germany (phone: +49 341 9940-2208; fax: +49 341 9940-2448; e-mail: kozlov@cbs.mpg.de) and with MR:comp GmbH, Gelsenkirchen, 45894, Germany.

G.M. Noetscher is with the Electrical and Computer Eng. Dept. at Worcester Polytechnic Institute, Worcester, MA 01604 USA (e-mail: gregn@wpi.edu).

A. Nazarian is with the Center for Advanced Orthopaedic Studies at Beth Israel Deaconess Medical Center, Harvard Med. School, Boston, MA (e-mail: anazaria@bidmc.harvard.edu).

S.N. Makarov is with the Electrical and Computer Eng. Dept. at Worcester Polytechnic Institute, Worcester, MA 01604 USA (e-mail: makarov@wpi.edu).

constant of 78 and conductivity of 0.48 S/m as a tool for heating investigations. However, the electrical properties of bone and muscle tissues surrounding the implant are significantly different from those values. Therefore, a question arises as to how well the corresponding simulation data obtained in concordance with ASTM F2182-11a correlate with similar data obtained for a realistic multi-tissue computational human model. The present paper aims to answer this question quantitatively.

Despite the fact that computer power and memory have increased significantly over the last few years, it is still a challenge to simulate complete design problems, i.e., a human model with realistic hip implants located inside a 1.5T MRI whole body radio frequency coil. A 3-D electromagnetics (EM) solver must provide robustness in handling complex coil and implant geometries, and a suitable human model should be available.

The use of a tetrahedral mesh variable in size results in very efficient meshing of the numerical domain. The recent introduction of high quality human models [3] suitable for a frequency domain solver allows one to perform reliable (without significant simplification) and relatively fast investigation of a human model with hip implants located inside a 1.5T MRI whole body RF coil.

Our goals in this study were: a) to develop a workflow for realistic implant modeling, which includes an MRI coil, a multi-tissue phantom, and accurately registered hip implants; b) to compute and report differences in the power loss density (PLD) rise generated due to the presence of three orthopaedic implants placed in the ASTM phantom or a realistic human model, located inside a 1.5 T coil.

II. METHOD

The MRI coil utilized was a 64 MHz high pass 16 rung birdcage design with dimensions relevant to clinical 1.5 T scanners: coils of diameter 604 mm and length 650 mm. The realistic 3-D EM model of the coil included all coil construction details for the resonance elements and the load (e.g. human body model or ASTM phantom), all simulated with precise dimensions and electrical material properties.

To mimic the clinical case, the coil was tuned and matched when loaded by a human multi-tissue model. This was done by using a 3-D EM and RF circuit co-simulation approach. The corresponding simulations of ASTM phantoms were done with values of fixed and variable capacitors obtained from the previous step [4].

We investigated 3-D EM and thermal behavior of three femoral implants acquired from the Center for Advanced

Orthopaedic Studies, BIDMC, Harvard Med. School (Fig. 1). They include: a) – Austin-Moore type implant (modular prosthesis with a separate ball head) without the top cap; b) – short proximal femoral nail with the proximal hip; c) – long proximal femoral nail with the proximal hip. The manufacturers' CAD data were not available. Therefore, the implants were scanned using a 3-D laser scanner at Natick Soldier Research, Development & Engineering Center, Natick, MA. The implant models were placed in a human model or the ASTM phantom.

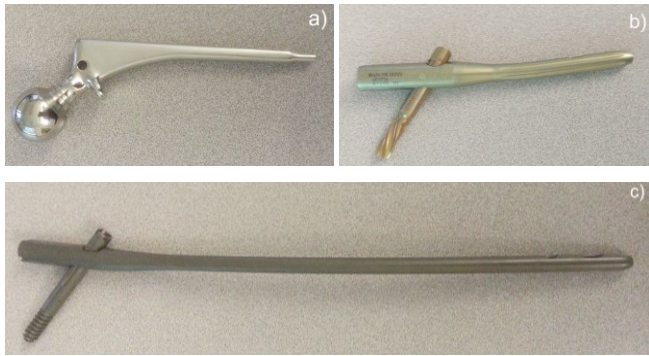


Figure 1. Photos of three implants investigated.

The load utilized was the multi-tissue VHP-Female v. 2.0 model [5] located at four landmark positions (Fig. 2). The model includes 130 individual tissue parts, in the form of finite-element triangular surface meshes with approximately 130,000 triangles total. Each tissue part has been extracted from the Visible Human Project®-Female dataset [6] of the National Library of Medicine using available cryosection images with a pixel resolution of 0.33 mm, providing state-of-the-art resolution of muscle and other soft tissues, as well as bone matter. Tissue electrical properties were defined as provided by the IT'IS Database for electromagnetic parameters of biological tissues [13].

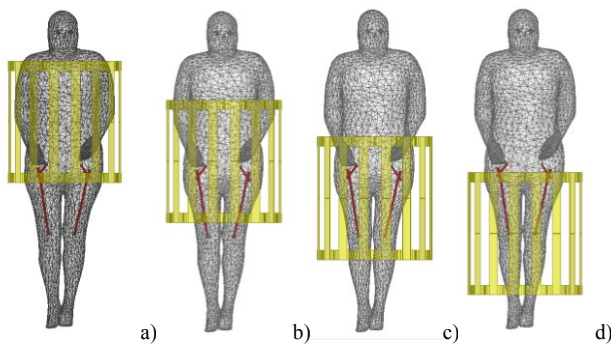


Figure 2. VHP model a selection of landmarks in the birdcage coil: a) -450 mm; b) -650 mm; c) -850 mm; d) -1050 mm

III. IMPLANT REGISTRATION

The implant registration enforces a proper implant size (vs. the size of the model bone), an anatomically correct implant position, and a certain part of the bone matter (cortical and/or trabecular) to be removed when necessary. A semiautomatic implant registration algorithm with a limited user intervention has been employed based on the principal idea to use at least two anchor nodes per implant: a fixed node and a floating node – see [7], [8]. The floating anchor node is a vertex of the implant mesh belonging to a certain

curve. An example is the floating anchor node in Fig. 3, which belongs to the long axis of the bone. The fixed anchor node is a joint coincident vertex of the femur mesh and the implant mesh. Originally, input meshes had an arbitrary orientation and position in space but we enforced that they were 2 manifold. These nodes define the proper implant position given the bone model and a cost function, with a “best fit” based on an intersection check [9] and the signed normal distances between implant/bone boundaries [10]-[12].

The suggested implant registration algorithm includes the following preliminary information: a) input data given in the form of two surface meshes: a Finite Element Method (FEM) surface mesh for a femur bone and a CAD model for an implant; b) an anatomically correct scaling routine formalized mathematically, which determines the required implant size given the femur size; c) at least one anatomically correct fixed anchor node per implant (Fig. 3); d) at least one anatomically correct floating anchor node per implant (Fig. 3); e) additional criterion – minimum thickness of the cortical bone matter with an embedded implant.

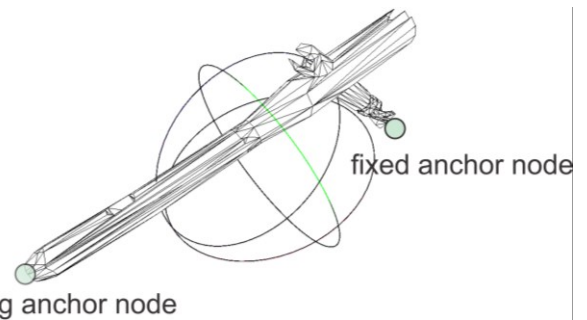


Figure 3. Anchor nodes and simplified implant CAD model of the short femoral nail.

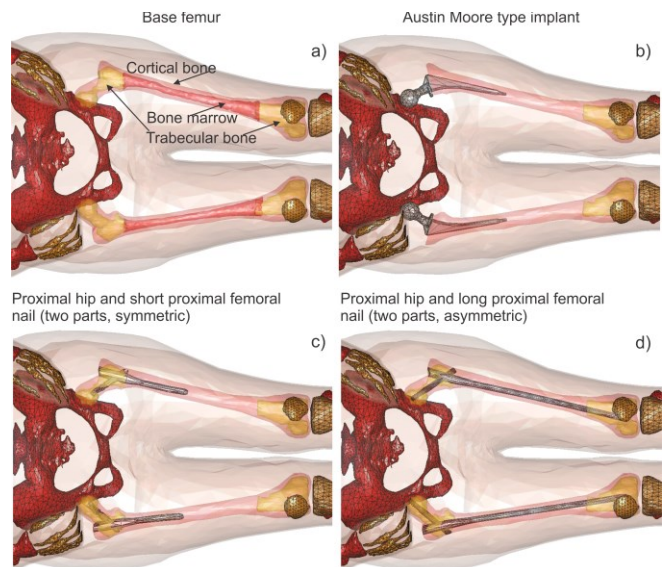


Figure 4. VHP-Female model and the three registered femoral implants.

A separate problem, which was solved after implant registration, was removing a part of the bone as required for a given implant. Figure 3 shows the original VHP-Female model (4a) and the three femoral implants registered within the model (4b, 4c, 4d). Only the hard tissues and the body shells (skin and fat) are shown. For the first hip implant in Fig. 4b, a gap of 0.5 mm exists between the cortical bone

matter and the implant which is filled with average body properties. The cancellous bone matter has been removed. For the second (short femoral nail) implant type in Fig. 4c, a gap of 0.5 mm also exists between the cancellous bone and the implant filled with the cortical bone matter. The implant is fully embedded within the cortical bone shell, which approximately models the effect of callus tissue formation around the implant tips. The last case of the long femoral implant in Fig. 4d has been treated similarly.

IV. RESULTS AND DISCUSSION

All 3D-EM ANSYS HFSS results were scaled for a transmit power of 2 W. This resulted in a whole body specific absorption ratio (wbSAR) of 0.0125 W/kg for the VHP model and of 0.031W/kg for the ASTM phantom.

PLD profiles in W/m^3 of selected simulations are presented in Figs. 6 – Fig. 9. Anticipated hot spots – areas with the largest PLD – were found close to either the implant tips, ends, or at both locations. The latter depended on the value of the incident tangential (to the long axis of the implant) electric field (E_{tan}), which was calculated without the presence of the implant, in these areas (Fig.5).

E_{tan} depends on human model topology, (e.g., body mass index, etc.) and MRI RF coil geometry (coil length, etc.). Further analysis should be conducted to cover diversity in the human population and MRI coil variety in order to make a final decision on if presence of a given implant does not cause harm to a person under MRI investigation.

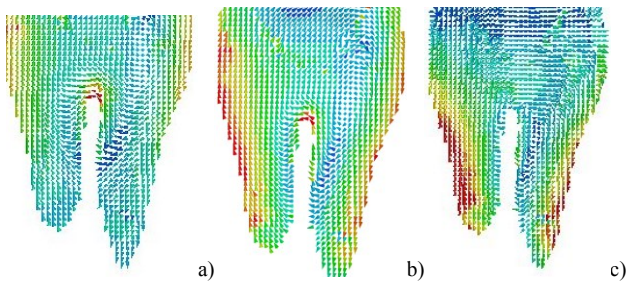


Figure 5. Vector electrical field profiles for the VHP model without implant at landmarks: a) -650 mm; b) -850 mm; c) -1050 mm

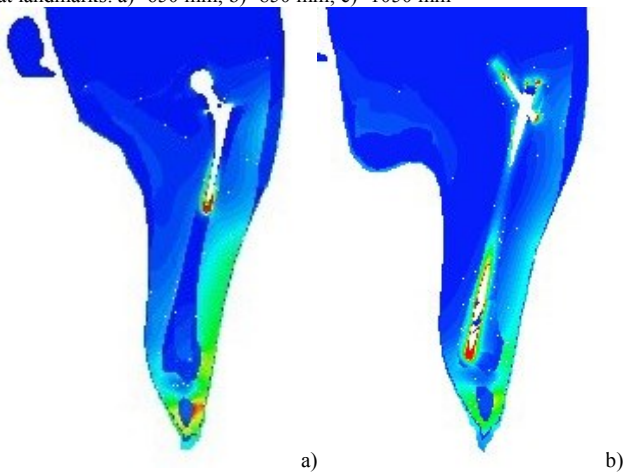


Figure 6. PLD profiles for the first and the third femoral implants registered in the VHP-Female model at landmark -1050mm. Color map max values: a) 300 W/m^3 , b) 500 W/m^3 . wbSAR=0.0125 W/kg

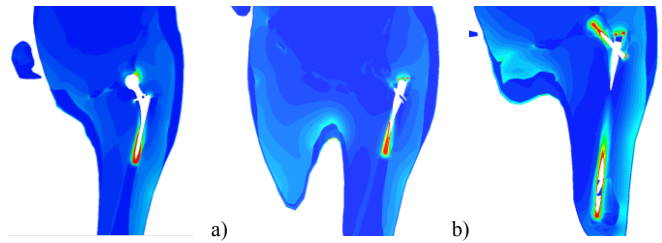


Figure 7. PLD profiles for the three femoral implants registered in the VHP-Female model at landmark -850mm. Color map max values: a) 600 W/m^3 , b) 800 W/m^3 , c) 500 W/m^3 . wbSAR=0.0125 W/kg

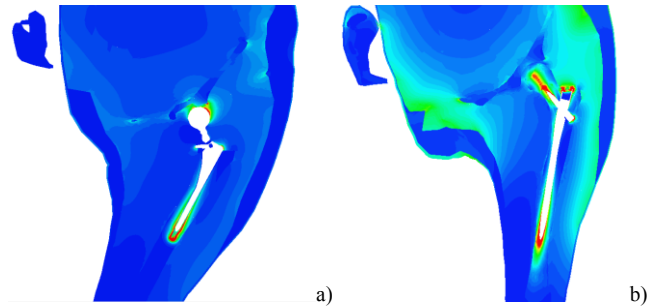


Figure 8. PLD profiles for the first and the third femoral implants registered with the VHP-Female model at landmark -650mm. Color map max values: a) 600 W/m^3 , b) 200 W/m^3 . wbSAR=0.0125 W/kg

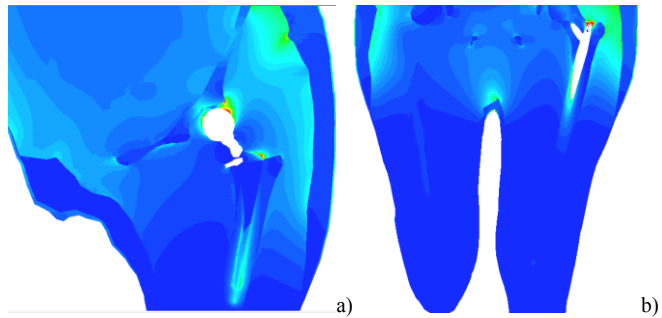


Figure 9. PLD profiles for the first and the third femoral implants registered with the VHP-Female model at landmark -450mm. Color map max values: a) 200 W/m^3 , b) 100 W/m^3 . wbSAR=0.0125 W/kg

Figure 10 shows selected ANSYS HFSS simulation results for PLD in a 1.5T whole-body RF coil and the ASTM phantom with the three implants located about ~ 20 mm from ASTM wall as prescribed by the ASTM F2182-11a standard. The PLD results for both VHP model and ASTM phantom demonstrated a certain qualitative agreement.

However taking into account that wbSAR is more than twice as large in the ASTM phantom, the quantitative correlation is poor for the third implant with an axial length was ~ 370 mm. That is essentially longer than the length (~ 150 mm) of ASTM phantom section where the distribution of E_{tan} is relatively homogeneous. Thus both implant tips and ends were located in an area where E_{tan} was essentially smaller than in the middle of the third implant.

The axial lengths of the first and second implants were ~ 150 mm. Thus these implants were excited by a homogeneous E_{tan} but this does not provide a guarantee that the given excitation would generate a PLD level that would be similar to the PLD for the human case.

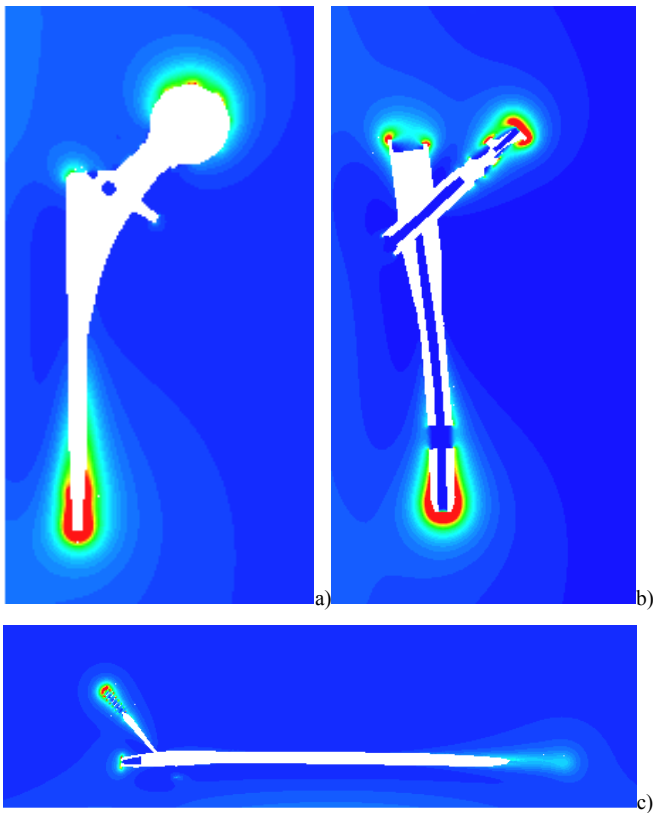


Figure 10. Power loss density for the three femoral implants located in ASTM phantom. Color map max value 1000 W/kg; $wbSAR=0.031W/kg$, $E_{tan}=19V_{p-p}/m$ averaged over 200 mm.

Figure 11 shows selected ANSYS HFSS – ANSYS Thermal co-simulation results for temperature rise inside the ASTM phantom with the three implants. Total thermal simulation time was 900 s with an initial time step of 0.001 s. Starting temperature was 22 °C. The thermal hot spot for the first implant was ~38% warmer than thermal hot spot for the second implant despite relative similar amplitudes of the PLD hot spots.

It is impossible to predict the peak value of the thermal hot spot for the human model case based on the ASTM phantom simulation case because the thermal properties of bone significantly differ from those of the ASTM high conductivity media. Unfortunately, an ANSYS HFSS – ANSYS Thermal co-simulation for the human model case is still a work in progress. We were not able to obtain thermal simulation results because (by default) the ANSYS thermal solver treats every finite-element triangular surface as a separated contact. This results in approximately 130,000 contact elements that make co-simulation time unacceptably long. The results on temperature rise for human model cases will be reported in the near future.

V. CONCLUSIONS

The present study provided differences in the power loss densities for the ASTM model and the realistic VHP-Female v. 2.0 human model located at different landmark positions, with three different types of embedded femoral implants, respectively. It is reasonably sufficient to raise doubt in the reliability of the test procedures described by the ASTM F2182-11a standard. However, it is not sufficient for final

conclusion of safety when considering patients with orthopedic metallic implants. Reliable 3-D EM thermal co-simulations should be accomplished for implants residing inside different human models located at different landmark positions with different MRI RF coils to assess a distribution of realistic temperature rise.

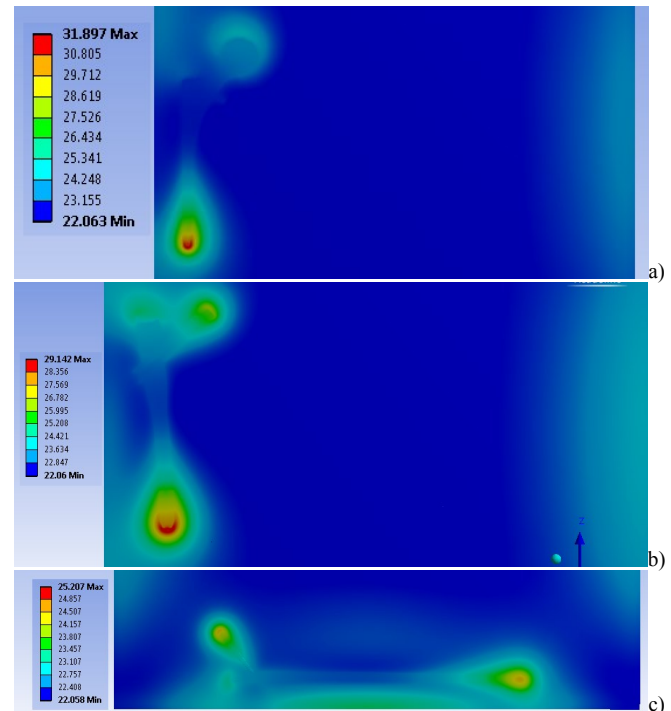


Figure 11. Temperature rise for the three implants located in ASTM phantom and oriented along Z axis; $wbSAR=3.1W/kg$, $E_{tan}=135V_{p-p}/m$

REFERENCES

- [1] M. Abbasi, G. Schaefer, J. D. Sánchez, and D. Erni, "Worst-Case Analysis of RF-Induced Heating During MRI Scanning in a Generic Multi-Component Orthopedic Medical Implant Applying the Design of Experiment Method (DoE)," *Joint Annual Meeting ISMRM-ESMRMB 2014*, 10-16 May 2014, Milan, Italy
- [2] H. Sanchez-Lopez, et. al, "Heating of bilateral hip prostheses in a human body model induced by a multi-axis gradient coil set," *Joint Annual MTG ISMRM-ESMRMB 2014*, 10-16 May 2014, Milan, Italy.
- [3] J. Yanamadala, et. al, "New VHP-Female v. 2.0 Full-Body Computational Phantom and Its Performance Metrics Using FEM Simulator ANSYS HFSS," *Proc. IEEE EMBC 2015*, Milan, 2015.
- [4] M. Kozlov, G. Schaefer, "Analysis of power deposition and temperature rise due to presence of an implant inside a 1.5T MRI RF coil," *Proc. IEEE EMBC 2015*, Milan, 2015.
- [5] Online: <https://www.nevaelectromagnetics.com/VHP2.html>.
- [6] U.S. National Library of Medicine. The Visible Human Project® Online: http://www.nlm.nih.gov/research/visible/visible_human.html.
- [7] Online: <http://ece.wpi.edu/ant/ImplantRegistration/movieRef6.avi>
- [8] Online: <http://ece.wpi.edu/ant/ImplantRegistration/movieRef7.avi>
- [9] T. Möller and B. Trumbore, "Fast, Minimum Storage Ray/Triangle Intersection," *J. of Graphics Tools*, vol. 2 (1997), pp. 21–28.
- [10] C. Ericson, *Real-Time Collision Detection*, New York:Elsevier, 2005.
- [11] M. W. Jones, *3D Distance from a Point to a Triangle*, Tech Report CSR-5-95, Dept. of Comp. Sci., Univ. of Wales Swansea, Feb. 1995.
- [12] D Eberly, *Distance Between Point and Triangle in 3D*, Technical Note, Geometric Tools, LLC, 20.
- [13] Haggall PA, Di Gennaro F, Baumgartner C, Neufeld E, Gosselin MC, Payne D, Klingeböck A, Kuster N, "IT'IS Database for thermal and electromagnetic parameters of biological tissues," Version 2.6, January 13th, 2015. www.itis.ethz.ch/database